Geophysical Journal International

Geophys. J. Int. (2017) **209,** 1585–1592
Advance Access publication 2017 March 16
GJI Seismology

doi: 10.1093/gji/ggx108

Dependence of seismic and radiated energy on shorter wavelength components

Shiro Hirano[1] and Yuji Yagi[2]

[1]*Department of Physical Science, College of Science and Engineering, Ritsumeikan University,* 1-1-1, *Nojihigashi, Kusatsu city, Shiga* 525-8577, *Japan. E-mail: s-hrn@fc.ritsumei.ac.jp*
[2]*Department of Earth Evolution Sciences, Graduate School of Life and Environmental Sciences, University of Tsukuba,* 1-1-1 *Tennoudai, Tsukuba city, Ibaraki* 305-8572, *Japan*

Accepted 2017 March 14. Received 2017 January 23; in original form 2016 July 5

SUMMARY

We discuss the theoretical estimation of co-seismic energy release with respect to a random spatial distribution of stress drop, which is an extension of conventional stress drop modelling. For slip distributions characterized by the von Kármán-type power spectral density, we examine the dependence of the estimated energy release on the upper limit and decay rate of the power spectral density in the shorter wavelength band. Using this dependence, we quantify the potential underestimation of energy release when the wavelength band limitation is not considered or the k^{-2} model is incorrectly assumed. Moreover, we discuss the estimation of radiated energy with respect to high-frequency components and suggest a relationship between stress drop heterogeneity and high-frequency radiation.

Key words: Inverse theory; Fractals and multifractals; Earthquake source observations; Theoretical seismology; Dynamics and mechanics of faulting.

1 INTRODUCTION

Co-seismic energy release can be modelled using physical quantities related to earthquake sources. Steketee (1958) and Savage (1969) derived a representation of energy release as an inner product of slip and stress on a fault surface; the derivation was subsequently improved by Andrews (1978). Although stress can be considered as a sum of the initial (tectonic) stress and co-seismic stress drop, the former is not observable. Therefore, we can consider only the inner product of slip and co-seismic stress drop within the framework of seismology. Here, this quantity is referred to as seismic energy, which has been interpreted as *'The energy of an earthquake'* (Kostrov 1974), *'The minimum estimate of strain energy drop'* (Kanamori 1977), or *'The available energy'* (Kanamori & Rivera 2006). In particular, Kanamori's (1977) description reveals the significance of this quantity.

A conventional method for estimating the seismic energy is to calculate the radiated energy because both slip and co-seismic stress drop can be identified when fracture energy on a fault is negligible (e.g. Ide & Beroza 2001). That is, if the critical slip-weakening distance is sufficiently smaller than the final slip distance. However, seismic inversion analyses have suggested that their ratio is 0.27–0.56 (e.g. Mikumo *et al.* 2003), and therefore, the fracture energy is not negligible. As such, the seismic energy and radiated energy must be estimated independently to understand the energetics of earthquakes.

Another method of estimation is to consider seismic energy as proportional to the product of seismic moment and average stress drop. This is valid for uniform stress drop along a fault (e.g. Aki 1966; Kanamori 1977). In such cases, seismic energy can be robustly estimated because the seismic moment depends only on the long- wavelengths of the spatial distribution of slip on a fault. In general, however, seismic energy depends on the entire spectrum of slip distribution if stress drop is heterogeneous along a fault, as described in the next section. Mai & Beroza (2002) analysed 44 slip models inferred by various authors and concluded that slip distributions on faults tend to follow the von Kármán-type random distribution, which is characterized by the Hurst exponent H that represents the decay rate of the larger wavenumber components of power spectral density (PSD). Accordingly, seismic energy should depend on the Hurst exponent, and the energy cannot be accurately estimated without considering higher wavenumber components.

In this study, we analytically quantify the dependence of seismic energy on higher wavenumber components of the von Kármán-type random slip distribution. Consequently, we also consider the dependence of radiated energy on the high frequency components. Moreover, we show a similarity and relation between the dependences. Hereafter, we refer to the higher wavenumber components and high-frequency components as shorter wavelength components.

2 THEORETICAL MODELLING AND RESULTS

In this section, we describe the modelling of seismic energy released by spatial slip patterns characterized by the von Kármán-type random distribution as a spectral integral. First, in Section 2.1, we describe an issue related to traditional concepts that assume a

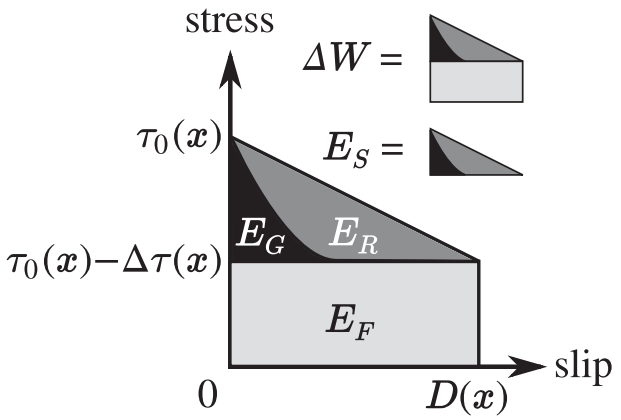

Figure 1. Schematic diagram of densities of the strain energy change ΔW, seismic energy E_S, radiated energy E_R, frictional heat E_F and fracture energy E_G at position $\boldsymbol{x}$ on the fault surface. Total amounts of each energy are defined as integrals of above densities with respect to $\boldsymbol{x}$.

homogeneous stress drop, which indicates the significance of shorter wavelength components. Next, in Section 2.2, we revisit Fractal Analysis by Circular Average, which simplifies the 2-D distribution with heterogeneity in a shorter wavelength band. Then, we derive the spectral integral in Section 2.3 and show that the integral is applicable to modelling radiated energy in Section 2.4.

2.1 Energy as a spectral integral

The magnitude of the co-seismic strain energy drop ΔW can be written as

$$\Delta W = \int_\Sigma D(\boldsymbol{x}) \left\{ \tau_0(\boldsymbol{x}) - \frac{1}{2}\Delta\tau(\boldsymbol{x}) \right\} \mathrm{d}\boldsymbol{x}, \tag{1}$$

where D, τ_0 and $\Delta\tau$ are the spatial distributions of the slip, initial stress, and stress drop at $\boldsymbol{x} = (x, y)$ on a fault surface Σ ($\subset \mathbb{R}^2$), respectively (e.g. Savage 1969). Seismologically, the initial stress is not observable; therefore, we can estimate only the seismic energy

$$E_S := \frac{1}{2}\int_\Sigma D(\boldsymbol{x})\Delta\tau(\boldsymbol{x})\mathrm{d}\boldsymbol{x}, \tag{2}$$

which is the second term of eq. (1) and provides a lower bound to ΔW. We summarize the contents of ΔW in Fig. 1. Although this type of figure has previously been shown by many authors (e.g. Kanamori & Brodsky 2004; Venkataraman & Kanamori 2004), we note that, generally, each area depends on the position $\boldsymbol{x}$ on the fault surface.

To calculate seismic energy, we must first estimate the slip distribution with a seismic inversion analysis and subsequently estimate the distribution of the stress drop. For simplicity, Aki (1966) and Kanamori (1977) assumed that the stress drop takes a uniform value $\Delta\tau_a$ on the fault, and derived the following equation

$$\begin{aligned} E_S &= \frac{\Delta\tau_a}{2}\int_\Sigma D(\boldsymbol{x})\mathrm{d}\boldsymbol{x} \\ &= \frac{\Delta\tau_a}{2\mu} M_0. \end{aligned} \tag{3}$$

The seismic moment M_0 predominantly depends on the longer wavelengths of the slip distribution, which is equivalent to the zero limit of the wavenumber in the Fourier domain, shown as

$$\begin{aligned} M_0 &= \mu \int_\Sigma D(\boldsymbol{x})\mathrm{d}\boldsymbol{x} \\ &= \mu \lim_{\boldsymbol{k}\to 0} \int_\Sigma D(\boldsymbol{x}) e^{i\boldsymbol{k}\cdot\boldsymbol{x}} \mathrm{d}\boldsymbol{x}, \end{aligned} \tag{4, 5}$$

where $\boldsymbol{k} = (k_x, k_y)$ is a wavenumber vector, and $\int D(\boldsymbol{x})e^{i\boldsymbol{k}\cdot\boldsymbol{x}}\mathrm{d}\boldsymbol{x}$ involves a 2-D Fourier transform of D. Assuming a uniform value of $\Delta\tau_a$ on the fault plane, E_S can be estimated without considering the shorter wavelength components of the fault slip distribution, which are difficult to resolve in seismic slip inversion.

In general, complexity of the slip distribution is a typical characteristic of earthquakes; therefore, complexity should be taken into account when estimating the seismic energy. For general distributions of slip and stress drop on a flat fault, the Plancherel theorem

$$\frac{1}{2}\int_\Sigma D(\boldsymbol{x})\Delta\tau^*(\boldsymbol{x})\mathrm{d}\boldsymbol{x} = \frac{1}{2}\int_{\mathbb{R}^2} \hat{D}(\boldsymbol{k})\Delta\hat{\tau}^*(\boldsymbol{k})\mathrm{d}\boldsymbol{k} \tag{6}$$

shows that shorter wavelength components are required, where $\hat{D}$ and $\Delta\hat{\tau}$ are 2-D Fourier transforms of D and $\Delta\tau$, respectively, and the asterisk indicates the complex conjugate. Assuming that (1) the flat fault is embedded in an infinite homogeneous medium, and (2) the slip vector is uniformly parallel to the x direction, Andrews (1980) derived the following

$$E_S = \int_{\mathbb{R}^2} \frac{\mu}{4k}\left(\frac{k_x^2}{1-\nu} + k_y^2\right)\left|\hat{D}(\boldsymbol{k})\right|^2 \mathrm{d}k_x\mathrm{d}k_y \tag{7}$$

from the right-hand side of eq. (6), where μ and ν are the rigidity and the Poisson ratio, respectively. Therefore, seismic energy depends on the PSD of the slip distribution.

2.2 FACA revisited

Mai & Beroza (2002) investigated PSD on the basis of 44 seismic inversion analyses. They executed the Fractal Analysis by Circular Average (FACA), which is a calculation of a circular integral of PSD of D in the wavenumber domain:

$$\int_{-\pi}^{+\pi} \left|\hat{D}(k,\phi)\right|^2 \mathrm{d}\phi, \tag{8}$$

where k and ϕ indicate the length and argument of $\boldsymbol{k}$, respectively. Originally, FACA was introduced for accurate estimation of the fractal dimension of computer-generated surfaces (Anguiano *et al.* 1994). Analyses of the fractal distribution can be simplified by this projection from a function of two variables to a function of one variable. Here, we clarify the meaning of this procedure and its advantage on the estimation of seismic energy.

FACA can be described as follows. For an isotropic 2-D function $f(\boldsymbol{x}) = f(r)$, where $r := |\boldsymbol{x}|$, its 2-D Fourier transform can be reduced to the Hankel transform:

$$\begin{aligned} f(\boldsymbol{k}) &= \int_{\mathbb{R}^2} f(\boldsymbol{x}) e^{-i\boldsymbol{k}\cdot\boldsymbol{x}}\mathrm{d}\boldsymbol{x} \\ &= 2\pi\int_0^{+\infty} f(r) r J_0(kr)\mathrm{d}r, \end{aligned} \tag{9, 10}$$

where J_0 is the Bessel function of the first kind. For a spectrum $\hat{D}(\boldsymbol{k})$ without the assumption of isotropy, the following holds:

$$\int_{-\pi}^{+\pi}\left|\hat{D}(\boldsymbol{k})\right|^2 \mathrm{d}\phi = \int_{-\pi}^{+\pi}\left\{\int_{\mathbb{R}^2} R_D(\boldsymbol{x}) e^{-i\boldsymbol{k}\cdot\boldsymbol{x}}\mathrm{d}\boldsymbol{x}\right\}\mathrm{d}\phi \tag{11}$$

$$= \int_0^{+\infty}\left\{\int_{-\pi}^{+\pi} R_D(r,\theta)\left\{\int_{-\pi}^{+\pi} e^{-ikr\cos(\theta-\phi)}\mathrm{d}\phi\right\}\mathrm{d}\theta\right\} r\,\mathrm{d}r \tag{12}$$

$$= 2\pi\int_0^{+\infty}\left\{\int_{-\pi}^{+\pi} R_D(r,\theta)\mathrm{d}\theta\right\} r J_0(kr)\mathrm{d}r, \tag{13}$$

where we use $J_0(x) = \int_{-\pi}^{+\pi} e^{-ix\cos\phi}\,\mathrm{d}\phi$, and the autocorrelation function is defined as

$$R_D(\boldsymbol{x}) := \int_{\mathbb{R}^2} D\left(\boldsymbol{x}'\right) D(\boldsymbol{x}'+\boldsymbol{x})\mathrm{d}\boldsymbol{x}', \tag{14}$$

and θ is an argument of $\boldsymbol{x}$. Hence, the circular average (8) is equivalent to the Hankel transform of the circular average of the autocorrelation function of D.

Next, we show the advantage of FACA in the estimation of E_S. Although the following argument was already implied by Andrews (1980) and Mai & Beroza (2002), it is worth showing it explicitly. The appendix of Mai & Beroza (2002) discusses the existence of the integral (7), where they explicitly assumed an isotropy of 2-D PSD $|\hat{D}(\boldsymbol{k})|^2$. However, their analysis of finite-fault slip models showed that the PSD was generally anisotropic, with longer correlation lengths along strike than down-dip. The discrepancy between the observations and the assumed PSD can be resolved in the following manner. After algebraic operations with the transformation of the wavenumber vector to the polar coordinate $(k_x,\ k_y) \mapsto (k\cos\phi,\ k\sin\phi)$ in eq. (7), we obtain the following:

$$I \le E_S \le \frac{I}{1-\nu}, \tag{15}$$

where

$$I := \frac{\mu}{4}\int_0^{+\infty}\left\{\int_{-\pi}^{+\pi}\left|\hat{D}(k,\phi)\right|^2 d\phi\right\}k^2\mathrm{d}k, \tag{16}$$

and the equality ($I = E_S$) is satisfied if and only if $\nu = 0$. In eq. (16), the integrand is already reduced to the isotropic function even if the PSD is anisotropic, such that the existence and the lower/upper bound of the energy can be discussed without the assumption of isotropy.

2.3 Seismic energy due to von Kármán-type PSD

We model I defined in eq. (16) as a function of some parameters that characterize the PSD of slip D. Mai & Beroza (2002) suggested the von Kármán-type PSD

$$\int_{-\pi}^{+\pi}\left|\hat{D}(\boldsymbol{k})\right|^2\mathrm{d}\phi = \frac{2\pi a_x a_z}{\left\{1+(k/k_c)^2\right\}^{1+H}} \tag{17}$$

for modelling of inversion results, where a_x and a_z are the correlation lengths in along-strike and downdip direction, respectively, and H is the Hurst exponent. As already highlighted by Mai & Beroza (2002), we should consider $H > 0.5$, otherwise, the integral (16) does not exist. For actual seismic inversion analyses, the wavenumber must have an upper limit, and we note this limit as k_{Max}. Hence, we assume that the PSD is obtained only within a range of $0 \le k < k_{\mathrm{Max}}$ and consider the following:

$$I(H, k_{\mathrm{Max}}) := \frac{\mu}{4}\int_0^{k_{\mathrm{Max}}} k^2\left\{\int_{-\pi}^{+\pi}\left|\hat{D}(\boldsymbol{k})\right|^2\mathrm{d}\phi\right\}\mathrm{d}k. \tag{18}$$

Taking the limit of $k \to 0$ for eq. (17), we obtain

$$\left|\hat{D}(0)\right|^2 = a_x a_z,$$

while

$$\hat{D}(0) = \lim_{\boldsymbol{k}\to 0}\int_\Sigma D(\boldsymbol{x})e^{i\boldsymbol{k}\cdot\boldsymbol{x}}\,\mathrm{d}\boldsymbol{x} = \int_\Sigma D(\boldsymbol{x})\,\mathrm{d}\boldsymbol{x}$$

holds. Thus, with the seismic potency $P := \int_\Sigma D(\boldsymbol{x})\,d\boldsymbol{x}$, by substituting eq. (17) into eq. (18), and after some algebra shown in Appendix A, we obtain

$$I(H, k_{\mathrm{Max}}) = \frac{\mu}{4}\int_0^{k_{\mathrm{Max}}}\frac{2\pi P^2k^2}{\left\{1+(k/k_c)^2\right\}^{1+H}}\mathrm{d}k \tag{19}$$

$$= \frac{\mu\pi}{4}P^2k_c^3B\left(K;\frac{3}{2},H-\frac{1}{2}\right), \tag{20}$$

where $K := \{1+(k_{\mathrm{Max}}/k_c)^{-2}\}^{-1}$, and an incomplete beta function is defined as follows:

$$B(x;a,b) := \int_0^x t^{a-1}(1-t)^{b-1}\,\mathrm{d}t. \tag{21}$$

Eq. (20) contains a relationship $E_S \propto L_c^3$, where L_c is a characteristic rupture length. This is because of $P \propto L_c^3$ and $k_c^{-1} \sim L_c$ (e.g. Causse *et al.* 2010). Moreover, eq. (20) can be compared to eq. (3) in view of the relation between E_S and seismic moment $M_0 = \mu P$ as follows:

$$\begin{aligned} E_S &\propto \mu P^2k_c^3B\left(K;\frac{3}{2},H-\frac{1}{2}\right)\\ &\propto M_0\overline{D}SL_c^{-3}B\left(K;\frac{3}{2},H-\frac{1}{2}\right)\\ &\propto \frac{\mu\overline{D}/L_c}{\mu}M_0B\left(K;\frac{3}{2},H-\frac{1}{2}\right), \end{aligned} \tag{22}$$

where $\overline{D}$ and S are averaged slip amount and the area of the fault, respectively, and satisfy $P = \overline{D}S$. In eq. (22), $\mu\overline{D}/L_c$ has the same dimension as $\Delta\tau_a$ in eq. (3). Hence, analogically, the incomplete beta function appears as a correction factor by which eq. (3) should be multiplied. In other words, apparent stress drop E_S/M_0 is affected by the shorter wavelength components via the incomplete beta function.

2.4 Radiated energy

Here, we show that the spectral integral of radiated energy E_R is similar to eq. (19). Let $\hat{\dot{M}}(f)$ be a spectrum of moment rate function, which is proportional to a far-field displacement spectrum $\hat{u}(f)$ in the case of frequency-independent attenuation. For these quantities,

$$E_R = \frac{8\pi}{5\rho}\left(\frac{1}{3\alpha^5}+\frac{1}{2\beta^5}\right)\int_0^{+\infty}f^2\left|\hat{\dot{M}}(f)\right|^2\mathrm{d}f \tag{23}$$

$$= C\int_0^{+\infty}f^2\left|\hat{u}(f)\right|^2\mathrm{d}f \tag{24}$$

holds, where α, β and ρ are the P-wave velocity, S-wave velocity and density, respectively, and C is a constant that depends on the internal structure of the Earth (e.g. Boatwright 1980; Venkataraman & Kanamori 2004). Moreover, a generalized model of $|\hat{u}(f)|$ has been suggested as

$$|\hat{u}(f)| = \frac{\hat{u}(0)}{\left\{1+(f/f_c)^{\gamma n}\right\}^{1/\gamma}}, \tag{25}$$

where f_c is the corner frequency, and γ and n are positive constants (Abercrombie 1995). The square of this spectrum is a generalized form of the von Kármán-type PSD (17), which is obtained by using $\gamma n = 2$ and $1/\gamma = (1+H)/2$. By substituting eq. (25) into (24) and after some algebra (Appendix A), we obtain the following:

$$\int_0^{f_{\mathrm{Max}}}f^2\left|\hat{u}(f)\right|^2\mathrm{d}f = \frac{1}{\gamma n}\hat{u}(0)^2f_c^3B\left(F;\frac{3}{\gamma n},\frac{2}{\gamma}-\frac{3}{\gamma n}\right), \tag{26}$$

where $f_{\rm Max}$ is the upper frequency limit and $F := \{1 + (f_{\rm Max}/f_c)^{-\gamma n}\}^{-1}$.

Comparisons of several observational data and eq. (25) suggest good fits for the case of $n = 2$ and $\gamma = 1$, which is known as the ω^{-2} model (e.g. Boatwright 1980; Abercrombie 1995; Mayeda & Walter 1996; Oth 2013). However, Abercrombie (1995) reported scattering of n values even after spectra correction taking the effect of Q into account. She proposed that this '*could result from the variation in the take-off angles of the rays with respect to the fault plane*' on the basis of a theoretical circular crack model (Madariaga 1976); this suggestion was confirmed and extended by the numerical calculations of Kaneko & Shearer (2014, 2015). Oth (2013) who parameterized the source spectra of 4188 events in Japan, carefully considering regional differences in attenuation and site response, which were then empirically corrected. Although almost all of the events follow the ω^{-2}-model, he suggested that the 2011 Tohoku earthquake (M 9.0) is an exception. Yagi *et al.* (2012) investigated the spectrum of moment rate function for the Tohoku earthquake. They stacked spectra for points distributed on the shallower and deeper parts of a fault and concluded that an asymptote of the spectra in the high-frequency band was $\sim f^{-2}$ for the shallower part and $\sim f^{-1.7}$ for the deeper part. In the deeper parts, rupture propagation and seismic radiation were strongly heterogeneous in view of the seismic energy release determined by the hybrid back-projection method (Yagi *et al.* 2012) and strong motion generation areas (Asano & Iwata 2012). This implies that the heterogeneous rupture style seen in the deeper parts of the Tohoku earthquake fault could generate spectra with ω^{-q} of $q \neq 2$. Therefore, the upper limit frequency and decay rate in the shorter wavelength band is important in order to estimate the appropriate seismic energy, especially for cases of such complex rupture.

3 INTERPRETATION AND DISCUSSION

3.1 Possible underestimation of E_S and E_R in a limited band

We introduce $R(H, k_{\rm Max}) := I(H, k_{\rm Max})/I(H, +\infty)$ to evaluate underestimation of E_S with band-limited ($0 \leq k < k_{\rm Max}$) information, and investigate its dependence on $k_{\rm Max}$ and H. We can discuss the degree of underestimation of E_R in the same manner by considering $k_{\rm Max}$ as $f_{\rm Max}$.

Plots of R are shown in Fig. 2, where a grey band of $4 < k_{\rm Max}/k_c < 22$ represents a range of $k_{\rm Max}/k_c$ for inversion analyses referred by Mai & Beroza (2002). In other words, PSD obtained in actual inversion analyses are limited below this band and, therefore, E_S may be underestimated due to lack of the shorter wavelength components. Assuming the ω^{-2} model, Ide & Beroza (2001) highlighted the following: *'integration up to approximately ten times the corner frequency is necessary to approach 90 per cent of the seismic energy'*. Note that *'the seismic energy'* in their context is E_R in our study because they consider both to be the same, and they estimated the energy on the basis of far-field spectra. For the von Kármán-type PSD, the ω^{-2} model is equivalent to the case of $H = 1.0$. A confirmation of their argument is shown in Fig. 2. For $H = 0.7$ and 0.8, however, the integrations up to $k_{\rm Max} = 10k_c$ are at most 55 per cent and 70 per cent of $I(H, +\infty)$, respectively, and severe underestimation will occur. Up to $k_{\rm Max} \sim 400k_c$ must be integrated for 90 per cent estimation of E_S if $H \sim 0.7$, which was obtained by Mai & Beroza (2002) as an averaged value.

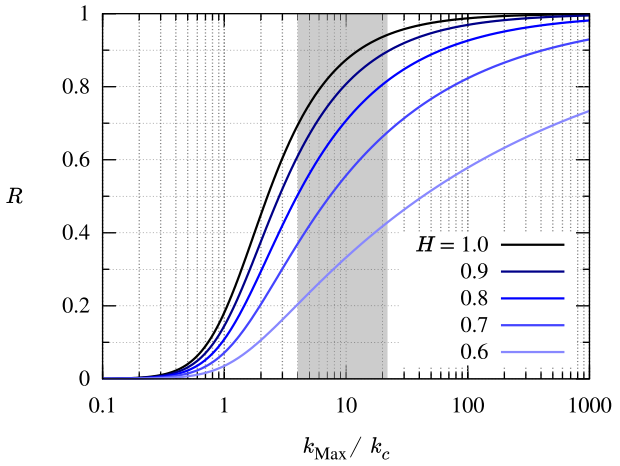

Figure 2. Plot of $R := I(H, k_{\rm Max})/I(H, +\infty)$. The light grey region indicates $4 < k_{\rm Max}/k_c < 22$ in which actual values of $k_{\rm Max}/k_c$ for inversion analyses are located (Mai & Beroza 2002).

3.2 Possible underestimation of E_S and E_R due to incorrect assumption of the k^{-2} or ω^{-2} model

Ide & Beroza (2001) proposed that the integral (24) can be calculated after an adjustment of spectra assuming the ω^{-2} model to estimate E_R. Although this scheme might be also applicable to the estimation of E_S, it might be underestimated if the shorter wavelength components of an actual spectrum are richer than the k^{-2} or ω^{-2} model. To this end, we define $R_H(H_1, H_2) := I(H_1, +\infty)/I(H_2, +\infty)$, and consider that H_1 and H_2 are assumed and true values of the Hurst exponent, respectively. For $H_1 = 1$, the numerator is an energy integral for the k^{-2} or ω^{-2} model, such that $R_H(1, H_2)$ represents the degree of underestimation when one incorrectly assumes the k^{-2} or ω^{-2} model. In the case of the averaged value, $R_H(1, 0.7) \sim 0.35$ is obtained (Fig. 3a). Accordingly, the energy integral up to a finite wavelength and the assumption of the k^{-2} and ω^{-2} models may be insufficient. Therefore, the effects of $k_{\rm Max}$ and H should always be estimated for the adjustment.

3.3 Application and approximation of $R_H(H_1, H_2)$

Here we suggest an application and useful approximation of the function $R_H(H_1, H_2)$ defined in the previous section. R_H can be helpful for evaluating not only underestimations but also errors in the estimation of energy. For example, let H be an estimated value of the Hurst exponent, and $\pm\epsilon$ be the error in the estimation due to some observational uncertainties. In this case, we can define the uncertainty of energy estimation as $R_H(H, H \pm \epsilon)$. We can pick an actual value of this function from Fig. 3(a) by assuming that $H_1 = H$ and $H_2 = H \pm \epsilon$; the point of $(H, H \pm \epsilon)$ is located at length ϵ from the line of $H_1 = H_2$ along the ordinate. Moreover, we find that $R_H(H_1, H_2)$ can be approximated by the following function:

$$R'_H(H_1, H_2) := \left(\frac{H_2 - 0.5}{H_1 - 0.5}\right)^{1.09}.$$

Fig. 3(b) shows $0.95 < R'_H/R_H < 1.05$ in $H_1 > 0.55$ and $H_2 > 0.55$, so that R'_H is a precise approximation of R_H in that range. With this function, we obtain

$$R_H(H, H \pm \epsilon) \sim \left(1 \pm \frac{\epsilon}{H - 0.5}\right)^{1.09}. \quad (27)$$

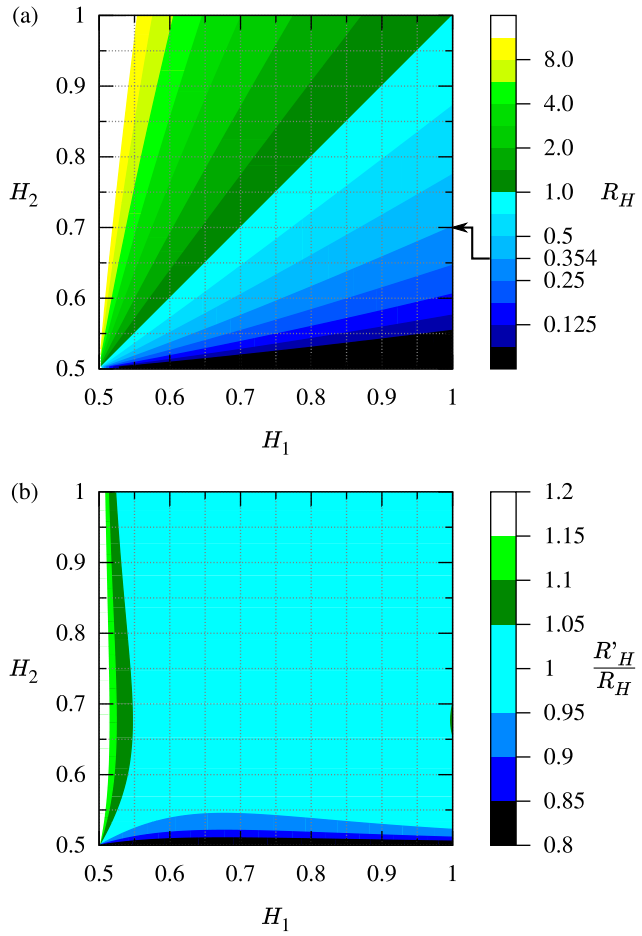

Figure 3. (a) Plot of $R_H := I(H_1, +\infty)/I(H_2, +\infty)$. The colour contour is in the log scale. The arrow indicates the point of $R_H(1, 0.7) \sim 0.354$. (b) Plot of R'_H/R_H.

Using eq. (27), we can easily evaluate the uncertainty in energy estimation after measuring the decay rate of the shorter-wavelength component and its error.

3.4 Practical problems and procedures for correction

The radiated energy E_R has been estimated for various earthquakes. For instance, Kanamori *et al.* (1993), Abercrombie (1995), and many other researchers directly calculated E_R using seismic waveforms and discussed the relationship between E_R and magnitude. Ide & Beroza (2001) carefully revisited the relationship after correcting missing spectra in the high-frequency band using the ω^{-2} model. Our result shows that spectra in the high-frequency band are necessary to estimate E_R accurately. Although seismic waves and moment rate functions are mostly approximated using the ω^{-2} model, in some cases their shorter wavelength components are richer than expected for the ω^{-2} model (Abercrombie 1995; Yagi *et al.* 2012). Moreover, spectra of slip distributions, which are required to calculate E_S, show similar characteristics; some of them obey the k^{-2} model while others do not (Mai & Beroza 2002).

This is important because underestimating E_R will affect estimation of the energy based magnitude. Previously, Choy *et al.* (2006) proposed $M_e := \frac{2}{3}\log_{10} E_R - 2.9$ as the definition of energy magnitude. On the basis of our results, however, such definitions of energy should be applied carefully. Here, we discuss possible errors in the estimation of energy magnitude.

If we denote the superscripts u and t for underestimated quantities and true quantities, respectively,

$$M_e^u - M_e^t = \frac{2}{3}\log_{10}\frac{E_R^u}{E_R^t} \tag{28}$$

holds, and R or R_H should be substituted into E_R^u/E_R^t according to their definitions. For example, $R_H(1, 0.7) \sim 0.35$ holds, which yields $\frac{2}{3}\log_{10} 0.35 \sim -0.3$. Hence, in this case, the energy magnitude could be $\sim$0.3 underestimated due to incorrect assumptions in the k^{-2} or ω^{-2} models. In general, radiated energy estimates would have large variability due to a range of uncertainties including the structure of the Earth, rupture velocity and directivity, etc. Additionally, the above value may suggest the significance of the Hurst exponent in energy estimation. Although the energy magnitude is important and helpful in evaluating the magnitude of tsunami earthquakes, possible errors due to incorrect assumptions of the Hurst exponent should be taken into account, as well as other uncertainties.

In cases where the spectrum $\hat{D}(k)$ or $\hat{\dot{M}}(f)$ does not obey the k^{-2} or ω^{-2} models, the energies E_S and E_R should be estimated by the following procedure: (1) confirm that the PSD is approximated by eq. (17) or (25) below the limit wavelength, and estimate the fall-off rate (i.e. H for E_S and n for E_R), (2) calculate the energy integral up to the limit wavelength (i.e. $I(H, k_{\mathrm{Max}})$), and (3) adjust the contribution of the shorter wavelength components (i.e. $I(H, +\infty) = I(H, k_{\mathrm{Max}})/R$). Step (1) has been performed occasionally (e.g. Abercrombie 1995; Mai & Beroza 2002; Yagi *et al.* 2012), but such analyses should be conducted more frequently. Moreover, steps (2) and (3) have been performed without (1) under the assumption of the ω^{-2} model by Ide & Beroza (2001). However, such methods should be modified because the effect of the fall-off rate is now clearly significant.

3.5 Relationship between E_S and E_R

The decay rate of the far-field spectrum is affected by, at least, attenuation (Abercrombie 1995), the take-off angle of rays (Madariaga 1976; Kaneko & Shearer 2014), and rupture directivity (Kaneko & Shearer 2015). In the following, we suggest that the decay rate is also affected by the heterogeneity of slip distribution characterized by the Hurst exponent. We consider a relationship between E_S and E_R via radiation efficiency $\eta_R := E_R/E_S = E_R/(E_G + E_R)$, where E_G is the fracture energy (e.g. Venkataraman & Kanamori 2004). On the basis of eq. (25) and the proportionality of $\hat{\dot{M}}(f)$ to $\hat{u}(f)$, we model the PSD of the moment rate function as

$$\left|\hat{\dot{M}}(f)\right|^2 = \frac{M_0^2}{\left\{1 + (f/f_c)^2\right\}^{2/\gamma}}, \tag{29}$$

where γn in eq. (25) is assumed to be two. We note that the right hand side of eq. (29) is approximated by $M_0^2/f^{4/\gamma}$ for $f \to \infty$. Originally, the asymptote of the square of the spectra in the high-frequency band is represented by $2n$ in eq. (25). However, in eq. (29), we describe the asymptote with $4/\gamma$ instead of $2n$ because this simplifies the comparison between energies based on eqs (17) and (25), as shown below. By substituting eq. (29) into (23), we obtain the following:

$$E_R \sim \frac{2\mu\pi}{5\beta^3} P^2 f_c^3 B\left(F; \frac{3}{2}, \frac{2}{\gamma} - \frac{3}{2}\right), \tag{30}$$

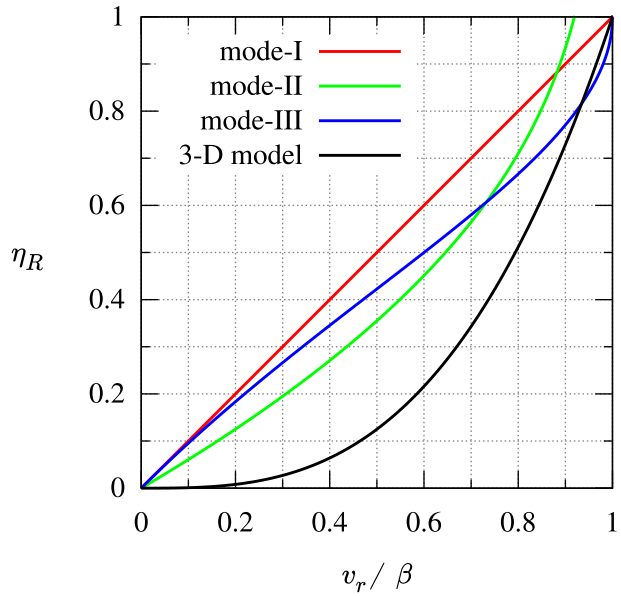

Figure 4. Dependence of the seismic efficiency η_R on normalized rupture velocity v_r/β. The black curve indicates both this study and Brune's 3-D circular crack model.

where we use $M_0 = \mu P$, $\mu/\rho = \beta^2$, and $(2/3)(\beta/\alpha)^5 \ll 1$. This representation and eq. (20) are reduced to

$$\eta_R \sim \frac{8}{5}\left(\frac{f_c}{\beta k_c}\right)^3 \frac{B\left(1; \frac{3}{2}, \frac{2}{\gamma} - 1 - \frac{1}{2}\right)}{B\left(1; \frac{3}{2}, H - \frac{1}{2}\right)} \tag{31}$$

for k_{Max}/k_c, $f_{\mathrm{Max}}/f_c \to +\infty$. Furthermore, we can assume that $f_c \sim v_r k_c$, where v_r is an averaged rupture velocity, because f_c and k_c are approximately equal to the inverse of the duration of the rupture process and the inverse of the length of the ruptured region, respectively. Finally, we arrive at the following approximation:

$$\eta_R \sim \frac{8}{5}\left(\frac{v_r}{\beta}\right)^3 R_H\left(\frac{2}{\gamma} - 1, H\right) \tag{32}$$

that includes two significant implications if H and γ are independent of v_r.

First, $\eta_R \propto (v_r/\beta)^3$ holds, which is equal to that of Brune's 3-D circular crack model with a uniform stress drop (see Appendix B). However, this is clearly different from the dependence of η_R on v_r for 2-D models (i.e. mode-I, mode-II, and mode-III sources) summarized by Venkataraman & Kanamori (2004) and plotted in Fig. 4. Hence, $\eta_R \propto (v_r/\beta)^3$ might be a common feature of 3-D models, and observed values should be compared to this dependence instead of the 2-D models applied by Venkataraman & Kanamori (2004).

Next, $R_H(2/\gamma - 1, H) \leq 1$ is required because $\eta_R \leq 1$ and $(8/5)(v_r/\beta)^3 \sim 1$ for $v_R/\beta > 0.8$. Fig. 3(a) shows that $R_H(2/\gamma - 1, H) \leq 1$ yields an inequality

$$\frac{2}{\gamma} - 1 \geq H. \tag{33}$$

This can be interpreted as follows. The amount of high-frequency components of $\dot{\hat{M}}(f)$ and $\hat{u}(f)$ decreases with increasing $2/\gamma - 1$. On the other hand, H increases with decreasing heterogeneity of the stress drop distribution. Moreover, the inequality (33) implies that $2/\gamma - 1$ increases with increasing H. Hence, we can conclude that faults with a smooth stress drop distribution may generate less high-frequency radiation. In other words, waves of high frequency are radiated by faults with strongly heterogeneous stress drop. This understanding will help in the estimation of source heterogeneity.

3.6 Future work to understand the effect of the Hurst exponent on the near- and far-field spectrum

The relationship (33) holds for the far-field spectra since we assume the proportionality of the moment-rate spectrum and the far-field spectrum. Regarding hazard assessment, the relationship between the Hurst exponent and the high-frequency decay rate of the near-field spectrum could be a concern. Such a relationship is, however, hard to analytically discuss because the relationship between the moment-rate spectrum and near-field spectrum is not simple. Moreover, even for the far-field spectrum, the decay rate can vary significantly depending on the direction of observation points (Kaneko & Shearer 2014) and rupture propagation (Kaneko & Shearer 2015). For further discussion on the physical backgrounds of observed spectra considering the heterogeneity of sources (i.e. the Hurst exponent), integration of analytical modelling and numerical simulations would be helpful and complementary. Mai & Beroza (2002) executed simulations and showed that, regardless of the fractal dimension of the heterogeneity, the high-frequency decay rate of the near-field spectrum is almost ω^{-2}. However, their work involved kinematic rupture simulations with a prescribed rupture velocity and source time function. Indeed, high-frequency radiation is efficiently generated due to perturbation of rupture velocity (e.g. Spudich & Frazer 1984), which is reproduced within a framework of spontaneous dynamic rupture simulations. Although a simulation of spontaneous rupture with heterogeneous stress drops and near-field ground motion was performed by Andrews & Ma (2016), the relationship between the rupture velocity perturbation and the Hurst exponent is still unknown because they only considered the case in which stress perturbation obeys the k^{-1} spectrum, which is equivalent to the k^{-2} model in terms of slip distribution. Hence, to investigate the relationship between H and observed spectra, dynamic spontaneous rupture simulations with heterogeneous stress drops and various Hurst exponents should be performed. After such simulations, our interpretation in the previous subsection based on analytical modelling will contribute to discussions of the physical background of this relationship.

4 CONCLUSIONS

We suggest unified representations of seismic energy E_S and radiated energy E_R, which are originally given as the spectral integral of the von Kármán-type PSD but can be finally reduced to the incomplete beta function. We confirm that the energies are severely underestimated if shorter wavelength components are neglected or the k^{-2} or ω^{-2} model is incorrectly assumed. We propose a procedure for correcting inaccurate estimates of the energies with respect to the fall-off rate of the PSD in the shorter wavelength band.

Available seismic data have become ever more abundant, and estimations and applications of earthquake-related energies have become even more important. However, data on shorter wavelength components are still lacking, which might be irrecoverable owing to attenuation and heterogeneity of the earth. In case of heterogeneous slip and stress drop, seismic energy strongly depends on the shorter wavelength components of the heterogeneity although it cannot be

resolved by seismic inversion analyses. Hence, we must treat the energies carefully by quantifying their accuracy.

ACKNOWLEDGEMENTS

This study was supported by The Mega Quake Risk Management project of Tsukuba University, Japan. We also appreciate helpful comments given by Xiaofei Chen, Paul Martin Mai and an anonymous reviewer.

REFERENCES

Abercrombie, R.E., 1995. Earthquake source scaling relationships from −1 to 5 M_L using seismograms recorded at 2.5-km depth, *J. geophys. Res.,* **100**(B12), 24 015–24 036.

Aki, K., 1966. Generation and propagation of G waves from the Niigata earthquake of June 16, 1964: Part 2. Estimation of earthquake moment, released energy, and stress-strain drop from the G wave spectrum, *Bull. Earthq. Res. Inst.,* **44**(1), 73–88.

Andrews, D.J., 1978. Coupling of energy between tectonic processes and earthquakes, *J. geophys. Res.,* **83**(B5), 2259–2264.

Andrews, D.J., 1980. A stochastic fault model 1: Static case, *J. geophys. Res.,* **85**(B7), 3867–3877.

Andrews, D.J. & Ma, S., 2016. Validating a dynamic earthquake model to produce realistic ground motion, *Bull. seism. Soc. Am.,* **106**(2), 665–672.

Anguiano, E., Pancorbo, M. & Aguilar, M., 1994. Pitfalls in the fractal characterization of real microscopic surfaces by frequency analysis and proposal of a new method, in *Fractals in the Natural and Applied Sciences,* pp. 37–46, ed. Novak, M.M., Elsevier Science.

Asano, K. & Iwata, T., 2012. Source model for strong ground motion generation in the frequency range 0.1–10 Hz during the 2011 Tohoku earthquake, *Earth Planets Space,* **64**(12), 1111–1123.

Boatwright, J., 1980. A spectral theory for circular seismic sources; simple estimates of source dimension, dynamic stress drop, and radiated seismic energy, *Bull. seism. Soc. Am.,* **70**(1), 1–27.

Causse, M., Cotton, F. & Mai, P.M., 2010. Constraining the roughness degree of slip heterogeneity, *J. geophys. Res.,* **115,** B05304, doi:10.1029/2009JB006747.

Choy, G.L., McGarr, A., Kirby, S.H. & Boatwright, J., 2006. An overview of the global variability in radiated energy and apparent stress, earthquakes: radiated energy and the physics of faulting, in *Geophysical Monograph Series 170,* the American Geophysical Union, doi:10.1029/170GM01.

Ide, S. & Beroza, G.C., 2001. Does apparent stress vary with earthquake size?, *Geophys. Res. Lett.,* **28**(17), 3349–3352.

Kanamori, H., 1977. The energy release in great earthquake, *J. geophys. Res.,* **82**(20), 2981–2987.

Kanamori, H. & Brodsky, E.E., 2004. The physics of earthquakes, *Rep. Prog. Phys.,* **67**(8), 1429–1496.

Kanamori, H. & Rivera, L., 2006. Energy partitioning during an earthquake, in *Geophysical Monograph Series 170,* the American Geophysical Union, doi:10.1029/170GM03.

Kanamori, H., Mori, J., Hauksson, E., Heaton, T.H., Hutton, L.K. & Jones, L.M., 1993. Determination of earthquake energy release and M_L using TERRAscope, *Bull. seism. Soc. Am.,* **83**(2), 330–346.

Kaneko, Y. & Shearer, P.M., 2014. Seismic source spectra and estimated stress drop derived from cohesive-zone models of circular subshear rupture, *Geophys. J. Int.,* **197**(2), 1002–1015.

Kaneko, Y. & Shearer, P.M., 2015. Variability of seismic source spectra, estimated stress drop, and radiated energy, derived from cohesive-zone models of symmetrical and asymmetrical circular and elliptical ruptures, *J. geophys. Res.,* **120**(2), 1053–1079.

Kostrov, V.V., 1974. Seismic moment and energy of earthquakes, and seismic flow of rock (translated to English), *Izv. Akad. Sci. USSR Phys. Solid Earth,* **1,** 23–44.

Madariaga, R., 1976. Dynamics of an expanding circular fault, *Bull. seism. Soc. Am.,* **66**(3), 639–666.

Mai, P.M. & Beroza, G.C., 2002. A spatial random field model to characterize complexity in earthquake slip, *J. geophys. Res.,* **107**(B11), 2308, doi:10.1029/2001JB000588.

Mayeda, K. & Walter, W.R., 1996. Moment, energy, stress drop, and source spectra of western United States earthquakes from regional coda envelopes, *J. geophys. Res.,* **101**(B5), 11 195–11 208.

Mikumo, T., Olsen, K.B., Fukuyama, E. & Yagi, Y., 2003. Stress-breakdown time and slip-weakening distance inferred from slip-velocity functions on earthquake faults, *Bull. seism. Soc. Am.,* **93**(1), 264–282.

Oth, A., 2013. On the characteristics of earthquake stress release variations in Japan, *Earth planet. Sci. Lett.,* **377–378,** 132–141.

Savage, J.C., 1969. Steketee's paradox, *Bull. seism. Soc. Am.,* **59**(1), 381–384.

Spudich, P. & Frazer, L.N., 1984. Use of ray theory to calculate high-frequency radiation from earthquake sources having spatially variable rupture velocity and stress drop, *Bull. seism. Soc. Am.,* **74**(6), 2061–2082.

Steketee, J.A., 1958. Some geophysical applications of the elasticity theory of dislocations, *Can. J. Phys.,* **36**(9), 1168–1198.

Udías, A., Madariaga, R. & Buforn, E., 2014. *Source Mechanisms of Earthquakes: Theory and Practice,* Cambridge Univ. Press.

Venkataraman, A. & Kanamori, H., 2004. Observational constraints on the fracture energy of subduction zone earthquakes, *J. geophys. Res.,* **109,** B05302, doi:10.1029/2003JB002549.

Yagi, Y., Nakano, A. & Kasahara, A., 2012. Smooth and rapid slip near the Japan trench during the 2011 Tohoku-oki earthquake revealed by a hybrid back-projection method, *Earth planet. Sci. Lett.,* **355–356,** 94–101.

APPENDIX A: CALCULATION OF EQS (20) AND (26)

In the following, $x, x_{\mathrm{Max}}, x_c, p$ and q are regarded as $k, k_{\mathrm{Max}}, k_c, 2$ and $1 + H$ for eq. (20) or $f, f_{\mathrm{Max}}, f_c, \gamma n$ and $2/\gamma$ for eq. (26). Deriving both sides of $s^p = t/(1-t)$ with respect to t, we get

$$\frac{\mathrm{d}s}{\mathrm{d}t} = \frac{1}{ps^{p-1}(1-t)^2}, \tag{A1}$$

which leads to the following calculation:

$$\int_0^{x_{\mathrm{Max}}} x^2 \left\{1 + (x/x_c)^p\right\}^{-q} \mathrm{d}x$$

$$= x_c^3 \int_0^{x_{\mathrm{Max}}/x_c} s^2 \left\{1 + s^p\right\}^{-q} \mathrm{d}s \tag{A2}$$

$$= x_c^3 \int_0^X s^2 \left\{1 + \frac{t}{1-t}\right\}^{-q} \frac{\mathrm{d}t}{ps^{p-1}(1-t)^2} \tag{A3}$$

$$= \frac{x_c^3}{p} \int_0^X s^{3-p} (1-t)^{q-2} \mathrm{d}t \tag{A4}$$

$$= \frac{x_c^3}{p} \int_0^X \left(\frac{t}{1-t}\right)^{\frac{3}{p}-1} (1-t)^{q-2} \mathrm{d}t \tag{A5}$$

$$= \frac{x_c^3}{p} B\left(X; \frac{3}{p}, q - \frac{3}{p}\right), \tag{A6}$$

where $s := x/x_c$, and $X := \left\{1 + (x_{\mathrm{Max}}/x_c)^{-p}\right\}^{-1}$.

APPENDIX B: RADIATION EFFICIENCY OF THE 3-D CIRCULAR CRACK MODEL

According to section 9.5.1 of Udías *et al.* (2014), E_R and E_S for the 3-D circular crack model, in which a uniform stress drop is assumed, are given as follows:

$$E_R \propto M_0^2 \left(\frac{f_c}{\beta}\right)^3, \tag{B1}$$

$$E_S = \frac{\Delta\tau_a M_0}{\mu}, \tag{B2}$$

where we use eq. (3) in this paper (note that E_R and E_S herein are written as E_S and ΔU, respectively, in Udías *et al.* 2014). Considering $M_0 \propto r^3$ and $f_c \sim v_r/r$, eqs (B1) and (B2) yield the following:

$$\eta_R \propto \frac{\mu}{\Delta\tau_a}\left(\frac{v_r}{\beta}\right)^3. \tag{B3}$$